Available online at www.sciencedirect.com
ScienceDirect
International Journal of Heat and Fluid Flow 29 (2008) 654–664
International Journal of HEAT AND FLUID FLOW
www.elsevier.com/locate/ijhff

Large-eddy simulation of variable-density turbulent axisymmetric jets

Ping Wang [a,*], Jochen Fröhlich [a], Vittorio Michelassi [b], Wolfgang Rodi [c]

[a] Institute of Fluid Mechanics, Technical University of Dresden, 01062 Dresden, Germany
[b] Nuovo Pignone, Via Felipe Matteucci 2, 50127 Florence, Italy
[c] Institute of Hydromechanics, University of Karlsruhe, 76128 Karlsruhe, Germany

Received 6 November 2007; received in revised form 5 February 2008; accepted 9 February 2008
Available online 18 March 2008

Abstract

Three cases of variable-density turbulent round jets discharging from a straight circular pipe into a weakly confined low-speed co-flowing air stream are studied with the aid of large-eddy simulation. The density ratios considered are 0.14 [Helium/air], 1.0 [air/air] and 1.52 [CO_2/air], with Reynolds numbers of 7000, 21,000 and 32,000, respectively. Detailed comparisons of the statistics show good agreement with the corresponding experiments. They confirm that a lower-density jet develops more rapidly than a denser jet with the same exit momentum flux. Pseudo-similarity behavior in the three variable-density round jets is well reproduced in the simulation. The coherent structures of the three jets are investigated by visualization of the iso-surface of pressure fluctuations and vorticity. In the developing stage of the Kelvin–Helmholtz instability, large finger-shape regions of vorticity are observed for the helium jet close to the nozzle lip. This feature, however, is not found in the air and the CO_2 jet. The occurrence of strong streamwise vorticities across the shear layer in the helium jet is demonstrated by a characteristic quantity related to the orientation of the vorticity.

Keywords: LES; Variable-density flow; Axisymmetric jet; Pseudo-similarity; Coherent structure; Streamwise vorticity

1. Introduction

Turbulent flows with variable density, which may be due to temperature variations stemming from reactions or variations in the composition by fluids of different density, exist widely in nature as well as in technical devices. The ability to predict the turbulent mixing in flows with variable density is vital for the modeling of the dynamics of such flows and a prerequisite for predicting turbulent combustion situations. Unlike the extensively studied jets with constant density, variable-density jets are less well understood. Relatively few experimental studies were reported for such cases. An experiment with helium/air mixture discharging into a confined swirling flow was carried out by Ahmed et al. (1985). Sreenivasan et al. (1989) performed an experimental study on round jets of different densities issuing into the ambient air. Their different densities were obtained by premixing helium and air in various proportions. About the same time, Monkewitz et al. (1989) and Monkewitz and Pfizenmaier (1991) carried out an experimental investigation of entrainment and mixing in transitional axisymmetric jets, where density difference were achieved by heating the air. Panchapakesan and Lumley (1993) conducted an experiment with helium injected into open quiescent air from a round nozzle. Later, Djeridane et al. (1996) and Amielh et al. (1996) performed experimental studies of variable-density turbulent jets, including helium, air and CO_2 jets exiting into a low-speed air co-flow. Numerical investigations of this type of flow are also relatively scarce. Jester-Zürker et al. (2005) performed a numerical study of turbulent non-reactive combustor flow under constant- and variable-density conditions using a Reynolds-stress turbulence model. They obtained good agreement between simulation and experiment for the constant-density flow, whereas the results for the variable-density flow were less satisfactory. Some large-eddy simulation (LES) of variable-density

* Corresponding author. Tel.: +49 351 46334910; fax: +49 351 46335246.
E-mail address: ping.wang@mailbox.tu-dresden.de (P. Wang).

0142-727X/$ - see front matter © 2008 Elsevier Inc. All rights reserved.
doi:10.1016/j.ijheatfluidflow.2008.02.002

round jets were also performed recently (Zhou et al., 2001; Tyliszczak and Boguslawski, 2006). To the authors' knowledge, however, detailed comparisons of LES results and experimental data for round jets, covering density ratios both lower and larger than unity, are not available in the literature.

The aim of the present work is to perform a detailed comparison of LES results and experimental data for three round jets with density ratios 0.14, 1.0, and 1.52 respectively, to gain a deeper understanding of the effect of density differences on the jet development.

2. Numerical method

In this study, the so-called low-Mach number version of the compressible Navier–Stokes equations is employed. With this approach, the pressure P is decomposed into a spatially constant component $P^{(0)}$, interpreted as the thermodynamic pressure, and a variable component $P^{(1)}$, interpreted as the dynamic pressure. $P^{(0)}$ is connected to temperature and density, while $P^{(1)}$ is related to the velocity field only and does not influence the density. Due to this decomposition, sonic waves are eliminated from the flow, so that the time step is not restricted by the speed of sound. The dimensionless low-Mach number equations read as follows:

$$\frac{\partial \rho}{\partial t}+\frac{\partial \rho u_i}{\partial x_i}=0 \tag{1}$$

$$\frac{\partial \rho u_i}{\partial t}+\frac{\partial \rho u_i u_j}{\partial x_j}=\frac{1}{Re}\frac{\partial \tau_{i,j}(\mu)}{\partial x_j}-\frac{\partial P^{(1)}}{\partial x_i} \tag{2}$$

$$\frac{\partial \rho c}{\partial t}+\frac{\partial \rho c u_j}{\partial x_j}=\frac{1}{ReSc}\frac{\partial}{\partial x_j}\left(\rho\alpha\frac{\partial c}{\partial x_j}\right) \tag{3}$$

$$\rho=F(P^{(0)},T,c) \tag{4}$$

where the symbols μ, ρ, u_i, T, c and α denote dynamic viscosity, density, velocity vector component, temperature, mass fraction of jet gas, and diffusion coefficient of jet gas into air, respectively, while $\tau_{i,j}(\mu)$ is the viscos stress. The symbol Re denotes the Reynolds number and Sc the Schmidt number. Eq. (4) represents the equation of state. For the three isothermal weakly confined jets studied in this work, $P^{(0)}$ and T are constant, so that the mixture density is determined only by the mass fraction c. Employing the ideal gas law, this reduces Eq. (4) to

$$\rho=\frac{P^{(0)}}{TR_u}\frac{M_{air}M_{gas}}{M_{gas}+c(M_{air}-M_{gas})} \tag{5}$$

where the symbols R_u, M_{air} and M_{gas} denote the universal gas constant, molecular weight of air and molecular weight of jet gas, respectively.

Applying large-eddy filtering to the low-Mach number equations, the corresponding filtered LES equations are obtained. The unclosed terms in these equations have to be determined by subgrid scale (SGS) models. The variable-density dynamic Smagorinsky model by Moin et al. (1991) is used to determine the SGS eddy viscosity, μ_T, in the momentum equations. The SGS scalar flux is modeled by the often-used gradient diffusion model:

$$\overline{\rho c u_j}-\bar{\rho}\tilde{c}\tilde{u}_j=-\frac{\mu_T}{Sc_T}\frac{\partial \tilde{c}}{\partial x_j} \tag{6}$$

where Sc_T is the turbulent Schmidt number. Sc_T may be determined with a dynamic procedure, as used for the SGS eddy viscosity (Moin et al., 1991). In this work it is set to $Sc_T=0.7$.

The simulations were performed with the in-house Finite Volume code LESOCC2C, which is a compressible version of LESOCC2 (Hinterberger, 2004). LESOCC2C is highly vectorized, and parallelization is accomplished by domain decomposition and explicit message passing via MPI. It solves the low-Mach number version of the compressible Navier–Stokes equations on body-fitted curvilinear block-structured grids employing second-order central schemes for the spatial discretization and a 3-step Runge–Kutta method for the temporal discretization. The convection term of the species equation was discretized with the HLPA scheme (Zhu, 1991).

3. Computational setup

Three jets issuing into a very slow co-flow of air are studied with density ratios equal to 0.14 [Helium/air], 1.0 [air/air], and 1.52 [CO_2/air], respectively (see Fig. 1). These cases correspond to situations studied experimentally by Djeridane et al. (1996) and Amielh et al. (1996). The parameters employed are listed in Table 1, in which the Reynolds number is based on the centerline velocity at the jet exit and the jet nozzle diameter The subscripts 'j' and 'e' relate to jet flow and external co-flow, respectively. It is worth noting that the momentum flux is the same for the three cases, $M_j=0.1N$. The reason for comparing cases with identical momentum flux is that in the flow region investigated inertial forces dominate (Djeridane et al.,

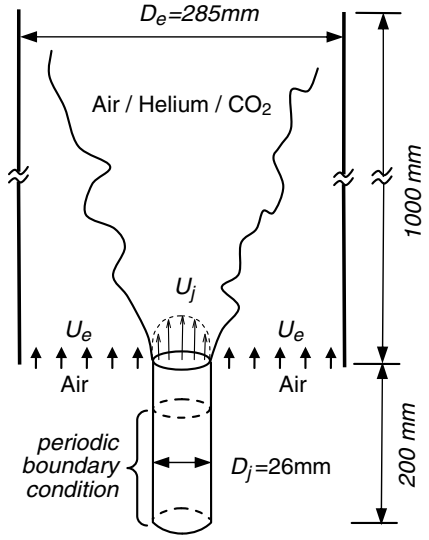

Fig. 1. Sketch of the computational domain.

Table 1
Parameters of the three jets simulated

Jet	ρ_j/ρ_e	U_j (m/s)	U_e (m/s)	Re_j	t_{aver}	Fr_j	X_1/D_j	X_2/D_j
Helium	0.14	32	0.9	7000	1285	654	7.8	78.0
Air	1.0	12	0.9	21,000	803	–	–	–
CO_2	1.52	10	0.9	32,000	1078	1147	18.8	188.0

1996; Amielh et al., 1996). The averaging time is given in units of D_j/U_j. Additional averaging was performed in azimuthal direction. Note that this is not effective near the axis so that the quality of averaging is better remote from the axis.

Fig. 1 shows a sketch of the flow configuration and the computational domain. The jet discharges from a long pipe into a co-flow confined by an outer pipe. The ratio of the pipe diameters is $D_e/D_j = 11$, so that the confinement is weak. The computational grid consists of 8 million cells, divided into 251 blocks. Fig. 2 provides related pictures. In the azimuthal direction 152 grid points are used and 385 grid points in axial direction from the outlet to the downstream end of the domain. The grid cells are stretched locally to reduce the cell size near the jet nozzle and across the shear layer. This resulted in a radial extent in wall units along the inner pipe wall of $\Delta r^+ = 3.0$, 8.0, and 10.5 for the helium, the air and the CO_2 jet, respectively. To perform a grid resolution study, a coarser grid consisting of 1 million cells was also employed.

A convective outflow boundary condition was imposed at the exit, and a uniform velocity profile without fluctuations at the inlet of the co-flow. Sensitivity studies were conducted imposing fluctuations in the inlet of the co-flow and a small boundary layer configured according to the experimental setup, but this did not have any effect on the computed statistics. In order to obtain a fully developed turbulent flow in the pipe upstream of the jet exit, as indicated by the experimental data, a separate simulation of turbulent pipe flow with streamwise periodic conditions was performed simultaneously (see Fig. 1). The Werner–Wengle wall function (Werner and Wengle, 1993) was used at the pipe walls.

The importance of buoyancy effects can be assessed by means of the exit Froude number Fr_j (Chen and Rodi, 1980), which is reported in Table 1,

$$Fr_j = \rho_j U_j^2/(g|\rho_j - \rho_e|D_j). \quad (7)$$

According to Chen and Rodi (1980), the vertical buoyant round jet behaves like a 'non-buoyant pure jet' in the region close to jet exit, where forces of inertia dominate over the forces of gravitation. This region extends up to X_1, which can be estimated as:

$$X_1 = 0.5 D_j Fr_j^{0.5} (\rho_j/\rho_e)^{0.25} \quad (8)$$

In the far field, which starts at $X_2 = 10X_1$, the jet behaves like a 'pure plume'. The values of X_1 and X_2 for the Helium jet and CO_2 jet are given in Table 1. Between these two regions $X_1 < x < X_2$ both forces are of similar importance. The length of the computational domain is $38.5\,D_j$ which, according to the values computed, covers the jet-like region and part of the intermediate region. The present study focuses on the region near the outlet so that, even if there possibly is a small upstream effect of the intermediate region, buoyancy forces can be neglected. A detailed discussion of this issue is also provided in Djeridane et al. (1996).

4. Comparison of statistical values

4.1. Profiles along the jet axis

A comparison of the axial evolution of mean streamwise velocity and mean mass fraction along the jet axis, U_c and C_c, is shown in Figs 3 and 4, respectively. The subscript 'c' denotes the value at the centerline in this context. Analyt-

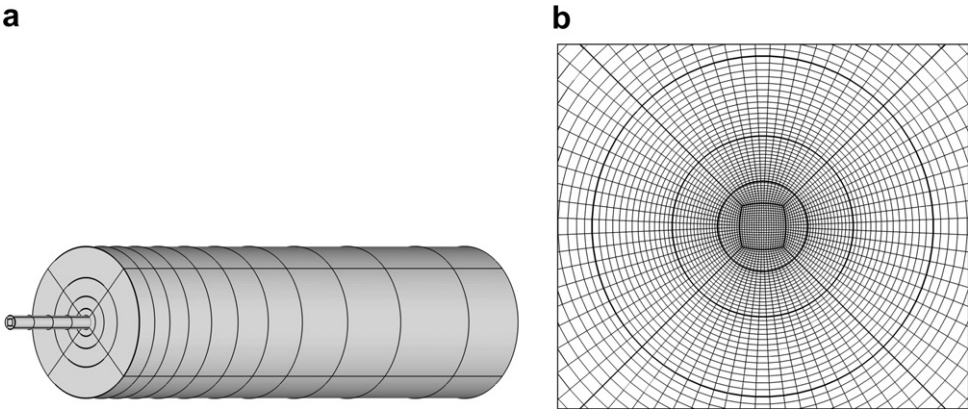

Fig. 2. (a) 3D view of the computational domain. Dark lines indicate block boundaries of the computational grid. (b) Zoom of the grid around the symmetry axis in a plane $x = \text{const.}$ (only every second point is shown).

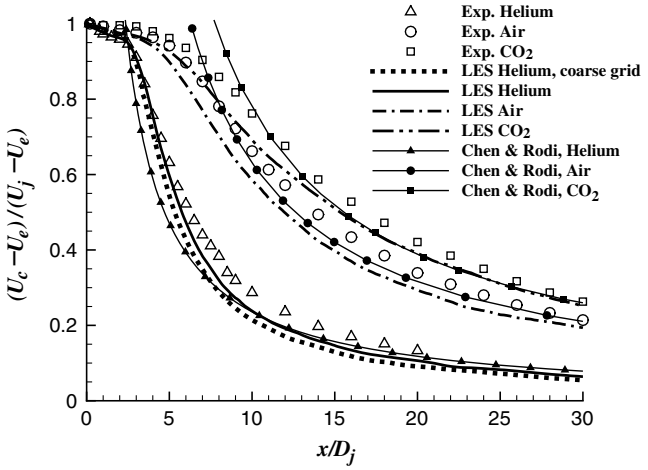

Fig. 3. Mean streamwise velocity along the jet axis. The similarity law proposed by Chen and Rodi (1980) is $U_c/U_j = 6.3(\rho_j/\rho_e)^{1/2}(D_j/x)$.

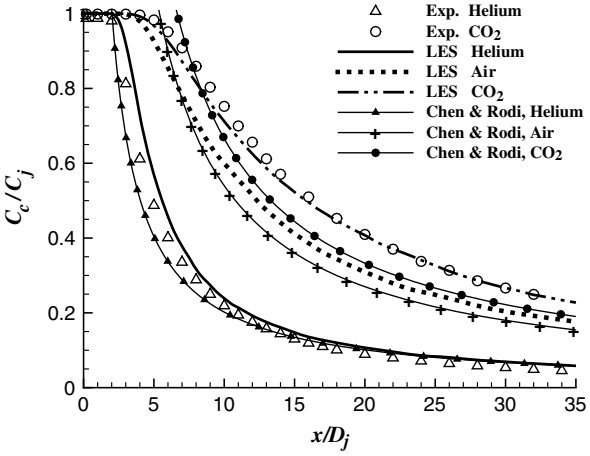

Fig. 4. Mean mass fraction along the jet axis. The similarity law proposed by Chen and Rodi (1980) is $C_c/C_j = 5.4(\rho_j/\rho_e)^{1/2}(D_j/x)$.

ical curves calculated from the similarity laws proposed for variable-density jets by Chen and Rodi (1980) are also included, which read as follows:

$$U_c/U_j = 6.3(\rho_j/\rho_e)^{1/2}(D_j/x) \quad (9)$$

$$C_c/C_j = 5.4(\rho_j/\rho_e)^{1/2}(D_j/x) \quad (10)$$

The influence of the density difference is obvious: the centerline velocity and concentration of the helium jet decays much faster than in the air and the CO_2 jet. Light gas, helium, tends to mix more rapidly with the ambient air than the heavier gases do (recall that the momentum flux is the same for all flows). This faster mixing of helium is accompanied by a faster increase of turbulence intensity in the near-nozzle region (see Fig. 5). The potential core of the helium jet is only 3 diameters long, much shorter than that of the air and CO_2 jet. Very good agreement between the LES results and the experimental data is obtained for the helium jet. For the heavier jets, some differences in the decay of U_c are observed. They might be due to a small mismatch of inflow conditions.

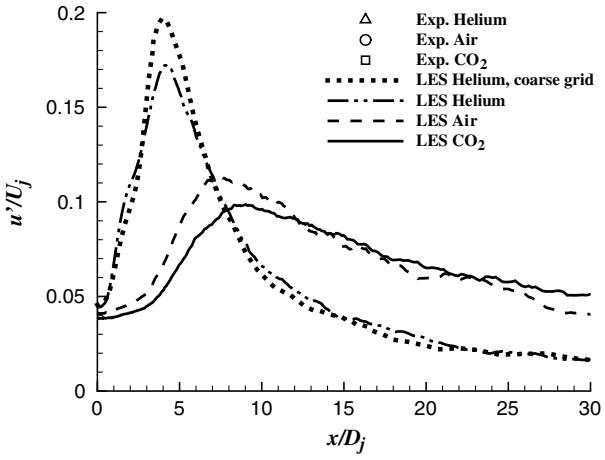

Fig. 5. Rms-fluctuations of the streamwise velocity component along the jet axis.

The influence of the density ratio ρ_j/ρ_e on the decay of U_c and C_c is also described quite well by the similarity laws, but no perfect agreement between the LES and these laws should be expected because the laws are only approximate, and in fact 'x' in the laws should be replaced by the distance from the virtual origin of the jet as a point source. To show the influence of grid resolution, the results for the helium jet obtained with the coarse grid are also displayed in Figs. 3 and 5.

The evolution of the rms-fluctuations of the streamwise velocity, u', along the jet axis is shown in Fig. 5. The influence of the density difference is obvious again: the helium jet decelerates much faster than the two heavier jets. At $x/D_j = 4.5$, the peak value of 17% for u'/U_j is already reached in the helium jet, whereas the peaks for the two heavier gases are lower, less pronounced, and attained further downstream. The fast increase of u'/U_j in the potential core region is due to the growth of the Kelvin–Helmholtz instability across the shear layer. Although the values of u'/U_j for the three jets at positions further downstream, for instance $x/D_j > 25$, are quite different, the values of $u'/(U_c - U_e)$, i.e. u' normalized with the local streamwise velocity difference, are close to each other and have a level of about 25–30%.

Fig. 6 shows the axial evolutions of the mean mass fraction half-width L_c, as well as the mean streamwise velocity half-width L_u for the different cases simulated. L_u is defined as the radius at which $U - U_e = 0.5(U_c - U_e)$, in order to take into account the co-flow effect. For $x/D_j > 10.0$, both LES results and experimental results show that: (1) the half-width increases approximately linearly; (2) L_c is always larger than L_u. The former hints to the existence of a similarity behavior, and the latter indicates that the scalar field always spreads faster than the velocity field. It is worth pointing out that, for the helium jet, the downstream values of L_u and L_c are very sensitive, because the profiles are very flat (see Figs. 7 and 10). According to Chen and Rodi (1980), the mean turbulent Schmidt

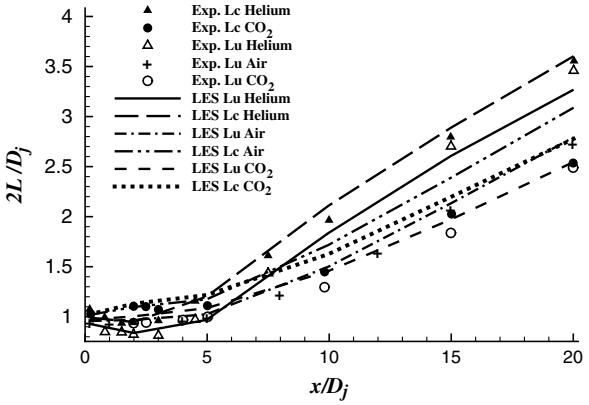

Fig. 6. Half-width of mean mass fraction and half-width of mean streamwise velocity along the jet axis.

number in the Reynolds averaged Navier–Stokes (RANS) framework $Sc_{T,RANS}$ is closely related to the square of the ratio L_u/L_c in the similarity region, and a value of $Sc_{T,RANS} = 0.7$ is recommended for round jets. Based on the values of L_u and L_c deduced from the LES data $Sc_{T,RANS}$ was computed using the same formula and values around 0.7 were found. Although Sc_T in Eq. (6) is only related to the SGS part of the concentration fluctuations it is not unreasonable to employ the RANS value for this purpose which was done in the present paper.

4.2. Radial distributions

The radial profiles of the normalized mean streamwise velocity U/U_j are shown in Fig. 7 for the helium and the CO_2 jet. The results of the air jet are close to those of the CO_2 jet. Very good agreement between LES and experiment is obtained for the helium jet. Starting from the typical turbulent pipe flow profile at $x/D_j = 0.2$, the centerline velocity of the jet decreases faster than for the CO_2 jet, as seen already from Fig. 3.

At the first station $x/D_j = 0.2$ in Fig. 7b, there is some disagreement for the CO_2 jet (see arrow). A reason may be that for this case the pipe flow was not fully developed at the exit in the experiment. Beyond $x/D_j = 0.2$, the agreement between LES and experiment is good also for the CO_2 jet.

The radial profiles of u', the rms-fluctuations of the streamwise velocity component, at several downstream positions are displayed in Fig. 8. Here, the local velocity half-width L_u is used for normalizing the radial coordinates, as in the experimental paper (Amielh et al., 1996). Again, very

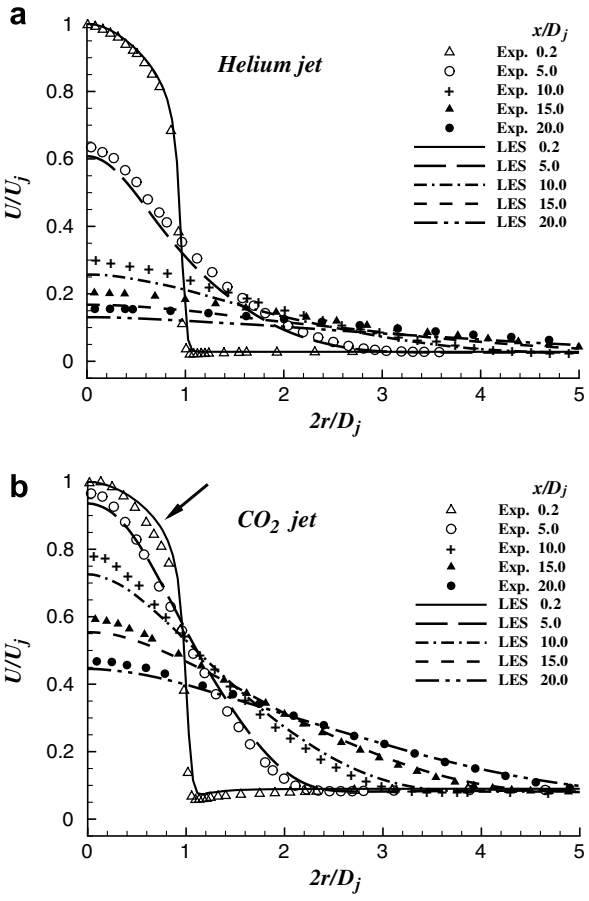

Fig. 7. Radial profiles of mean streamwise velocity at several axial positions.

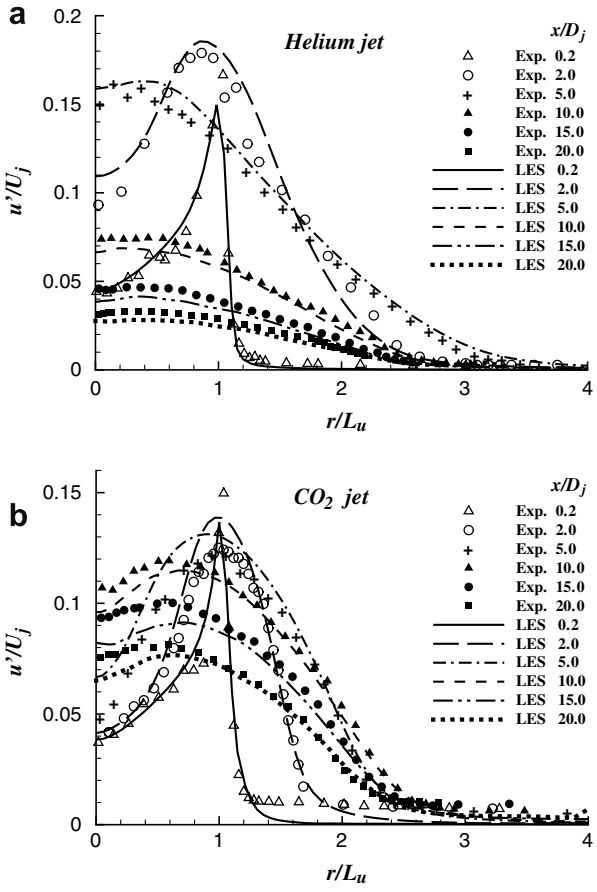

Fig. 8. Radial profiles of streamwise rms-fluctuations.

good agreement is obtained for the helium jet. At the location very close to the jet nozzle, $x/D_j = 0.2$, both jets show a peak value of 0.15 in the shear layer and a value of 0.04 on the axis. Further downstream, the peak of the u' profiles moves to the center and the value of u' on the axis increases due to mixing processes. Finally, the profiles reach an approximately self-similar shape. Fig. 8 shows that this transition is much faster for the helium jet than for the CO_2 jet.

Radial distributions of the normalized Reynolds shear stress $\langle u'v'\rangle/U_j^2$ are plotted in Fig. 9. With the two jets, different scales are used for the vertical axes for clarity. The agreement for the helium jet is excellent. In Fig. 9a, the peak of $\langle u'v'\rangle/U_j^2$ at the first section $x/D_j = 0.2$ is only 0.003. Further downstream at $x/D_j = 2.0$, the maximum is almost four times as large and the shape of the curve is substantially smoother. At even larger x/D_j, the shear stress decays again due to the broadening of the jet and the resulting reduction of gradients. The results for the CO_2 jet in Fig. 9b show a substantially stronger peak in the shear stress right at the outlet which is extremely difficult to capture. At $x/D_j = 2.0$ and 5.0, the computed profiles have the correct shape but exceed the experimental data by about 25%. Further downstream, the agreement is very good. The reasons for the differences observed may reside in an under-resolution of the very first stages of the initial development. Actually a mean turbulent viscosity of $\mu_T \approx 2.4\mu$ is observed in the shear layer of the CO_2 jet, while in the Helium jet $\mu_T \approx 0.5\mu$. This is because the Reynolds number for the CO_2 jet is higher than for the Helium jet.

The radial profiles of the mean mass fraction at several downstream positions are shown in Fig. 10. It is seen that, in the potential core region i.e. at the section $x/D_j = 0.2$, the 'top-hat' profiles are almost identical for the two jets. The radial profiles of mean mass fraction develop faster for the helium jet in the downstream direction. A very good agreement is obtained for the helium jet. For the CO_2 jet, however, systematic offset was observed between the LES data and the original experimental data at $x/D_j = 15.0$. The present authors then detected a slight inconsistency in the published experimental data, in that the values of the mass fraction on the centerline do not always agree when comparing the data for $r = 0$ with those for $x = \text{const}$. For this reason the experimental profile of the mean mass fraction for the CO_2 jet at section $x/D_j = 15.0$ plotted in Fig. 10b was obtained from the profile shown in Djeridane et al. (1996) by rescaling it with the C_c value extracted from Fig. 4. The resulting agreement then is very good, bearing in mind the confinement effect discussed below.

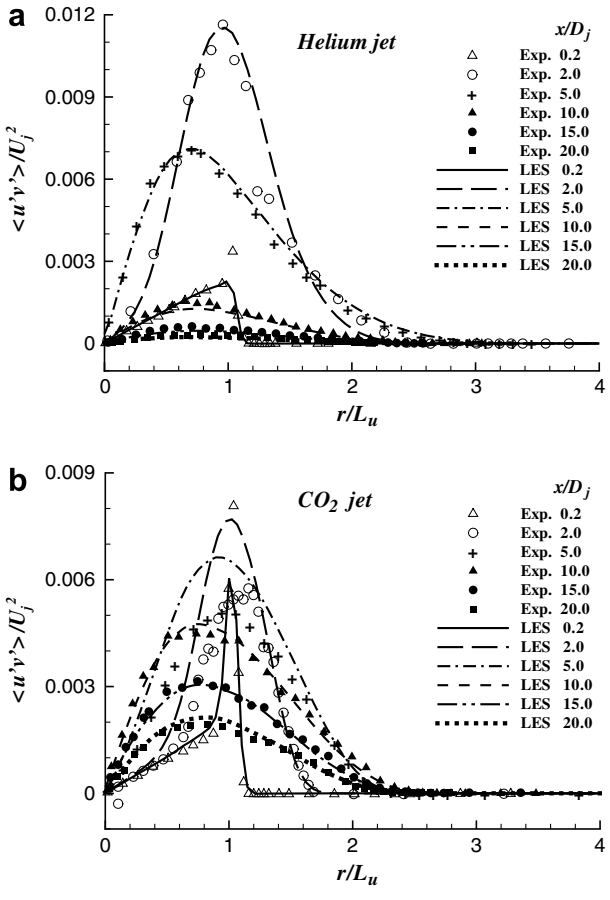

Fig. 9. Radial profiles of shear stress $\langle u'v'\rangle/U_j^2$.

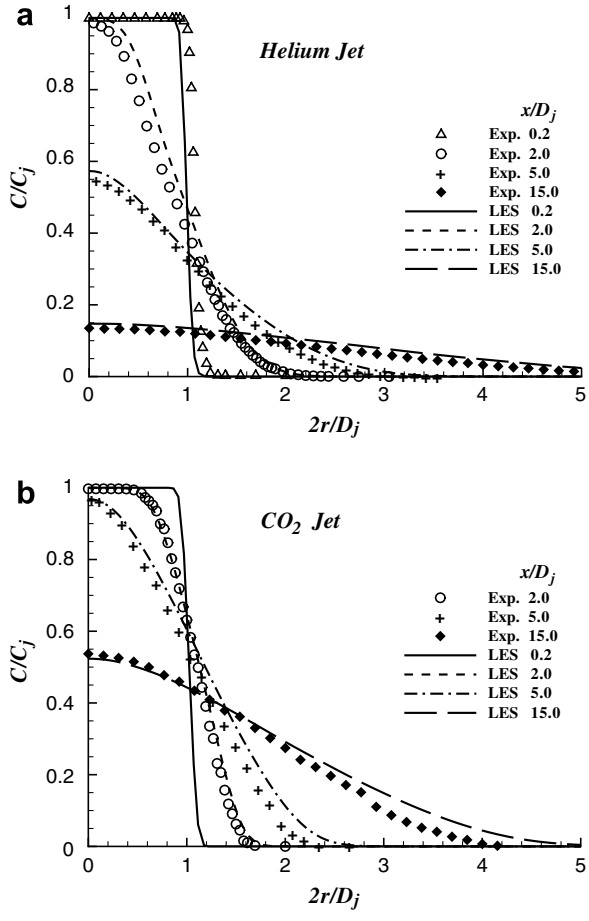

Fig. 10. Radial profiles of mean mass fraction.

4.3. Pseudo-similarity

Self-similarity can be found in many turbulent flows, of which the constant-density jet is one example. In variable-density turbulent jets, approximate self-similarity exists in some regions, as discussed by Chen and Rodi (1980), so that the term pseudo-similarity is used here. One of these regions is the near field, where buoyancy forces are negligible compared to inertial forces. The current results mainly pertain to this region so that pseudo-similarity can be expected.

Radial profiles of the mean streamwise velocity and the mean scalar concentration normalized by the values at the jet axis are shown in Fig. 11 for several axial positions. For each curve, the reference length is the local half-width of the respective quantity. The computed and the measured profiles collapse fairly well. These curves are well represented by a Gaussian function, except for the mean scalar fraction at the positions far downstream near the outer edge ($r/L_c > 1.4$). This is due to the confinement starting to have an effect (Djeridane et al., 1996). The good collapse of the radial profiles and the approximately linear increase of the half-width (see Fig. 6) demonstrate the validity of pseudo-similarity in the present variable-density jets.

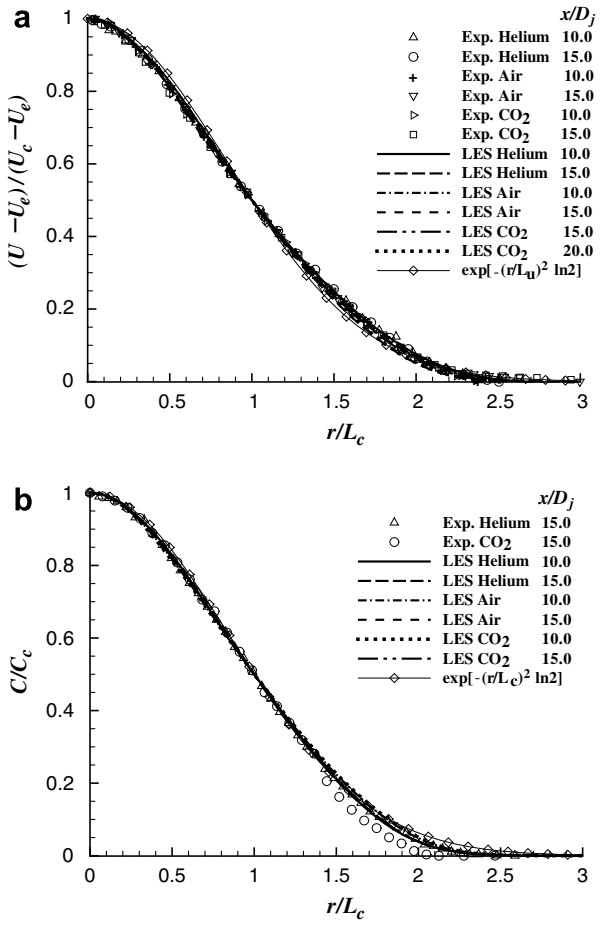

Fig. 11. Similarity profiles of mean streamwise velocity and mean mass fraction.

5. Coherent structures

Many investigations have been carried out and aimed to explain the faster mixing and entrainment in the lighter jets (Monkewitz et al., 1989; Monkewitz and Pfizenmaier, 1991; Fulachier et al., 1989). By flow visualization in hot air jets, Monkewitz et al. (1989) found a star-shaped jet cross section with two to six radial fingers in the potential core region. These fingers, which they called 'side jets' in this context, significantly increase the spreading angle, and it was concluded that the 'side jets' are generated by the so-called Widnall instability (Widnall et al., 1974). This mechanism is relevant for the azimuthal instability of vortex rings. In a later experimental investigation, however, Monkewitz and Pfizenmaier (1991) revised the previous conclusion. By checking the phase-averaged axial and radial velocities, they concluded that strong streamwise vortex pairs on the braids between the vortex rings are as important for the generation of 'side jets' as the Widnall instability. Gharbi et al. (1995) performed a statistical analysis of the jets considered here. They concluded that the structure of turbulence downstream and in the outer region is similar in all cases while in the near field the properties strongly depend on the density ratio.

The present LES data allow to investigate the formation and evolution of coherent structures, which are responsible for the lager-scale exchange of mass and momentum. Iso-surfaces of the pressure fluctuation $p-\langle p\rangle$ are employed for this purpose, as successfully used already with swirling constant-density jets by García-Villalba et al. (2006). Like in this previous work, a 3D box filter of twice the step size of the grid is used for smoothing in a post-processing step in order to enhance the clarity of the picture. Fig. 12 shows such instantaneous iso-surfaces for the helium, the air and the CO_2 jet, respectively. For optimal presentation of the structures, the constant value for obtaining the iso-surface was slightly adjusted in each case, but all values are very close to zero. Shortly downstream of the nozzle, vortex rings are observed in all the three jets due to the KelvinHelmholtz instability. Further downstream in the air jet, larger structures form at the outer edge of the jet. In the CO_2 jet, the behavior is similar to the air jet, but the distance between the vortex rings appears to be shorter and the intermittency lower. For the helium jet in contrast, the vortex rings seem to have a larger distance and a larger size. These observations are made in the near-field region where an inner core and a surrounding flow can be distinguished. In Fig. 12 this would be up to $x/D_j \approx 10, 14, 18$ for the helium, air, and CO_2 jet, respectively (lighter jets develop faster as discussed above). Beyond this region, the turbulent motion seems to be fairly homogeneous and vortex rings or similar structures can no longer be discerned.

Fig. 13 is concerned with the close vicinity of the jet outlet. It shows iso-surfaces of the vorticity modulus for the three jets in this region. In the following vorticity is normalized with the diameter of the pipe D_j and the centerline

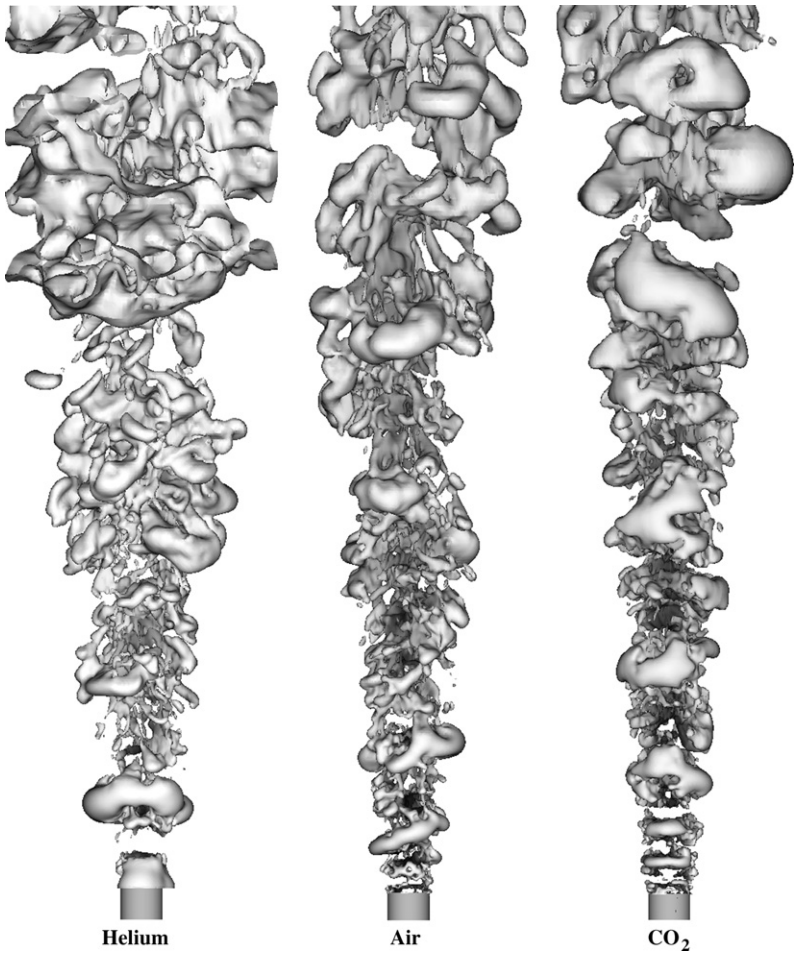

Fig. 12. Iso-surfaces of pressure fluctuation.

velocity of the jet at the outlet U_j. The maximum of the vorticity modulus in these units is approximately 15.0 for all cases. In the helium jet, large vortices are found which are regularly arranged along the lip. The length of these fingers is about one diameter. On the contrary, in the air and the CO_2 jet, only fairly continuous vortex sheets can be seen at the lip of the nozzle, the length of which is shorter. Since the finger-shape structures in the helium jet are approximately parallel to the jet axis, it is reasonable to believe that strong streamwise vorticity is present across the shear layer close to the lip. The streamwise vorticity in the helium jet is mainly generated by the Rayleigh–Taylor instability. This secondary instability developing in variable-density flows has been studied extensively (Schowalter et al., 1994; Reinaud et al., 1999). Schowalter et al. (1994) showed that spanwise vortices generate streamwise vorticity if in a stratified shear layer a lighter fluid drives the heavier fluid.

Fig. 14 shows several snapshots of ω_x and $(\omega_y^2+\omega_z^2)^{0.5}$ at three axial cross sections at the vicinity of the jet outlet. In each picture, a black circle is drawn to represent the location of the nozzle lip. It is found that the in-plane vorticity, denoted by $(\omega_y^2+\omega_z^2)^{0.5}$, is generally slightly larger for the helium jet than for the CO_2 jet. The shear layer is fairly circular upstream, but develops more and more wrinkles further downstream. Together with the wrinkling of the shear layer streamwise vorticity is generated. It is also seen that these streamwise vorticities in the helium jet are stronger than in the CO_2 jet.

In order to investigate the orientation of vorticity with respect to the jet axis the following characteristic quantity is computed:

$$\Omega_{x/yz} = |\omega_x|/(\omega_y^2+\omega_z^2)^{0.5} = \mathrm{arc\,tg}(\varphi) \tag{11}$$

where φ is the angle between the vorticity vector and the y–z-plane. Fig. 15a shows the average value of this quantity in the center plane (averaging is performed both in time and in azimuthal direction). For the helium jet, the change towards the free stream at the outer edge is somewhat broader which reflects the faster mixing of the helium jet. In the center and near the nozzle, a cone-shaped region with value around 0.8 exists in all three jets. It is closely related to the potential core region. An interesting difference among these figures is found in the initial developing region of the shear layer. Fig. 15d–f shows close ups of this region. It is seen that a region with high values exists just beside the shear layer in the helium jet (see Fig. 15d), but not in the air

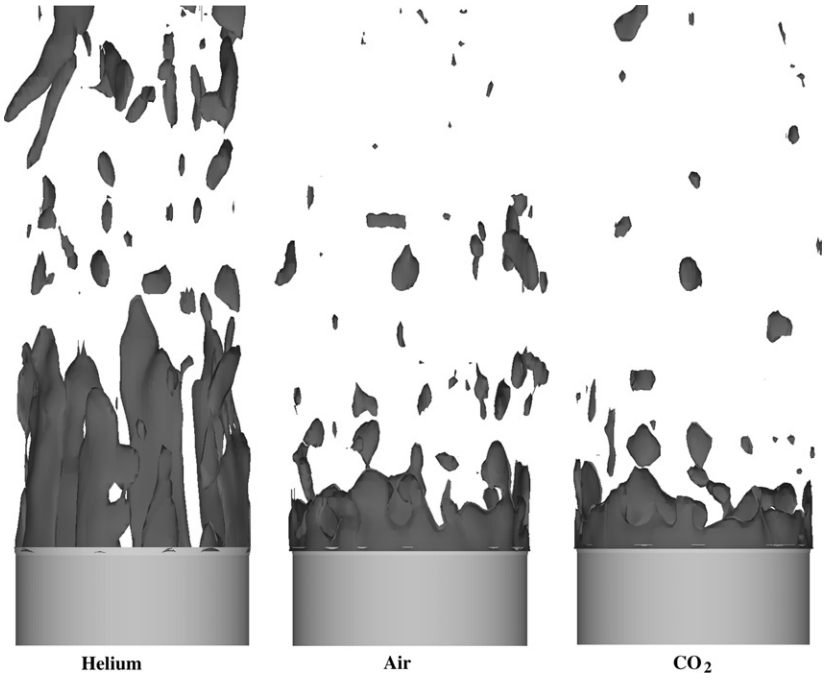

Fig. 13. Iso-surfaces of the vorticity modulus, $|\omega| = 9$.

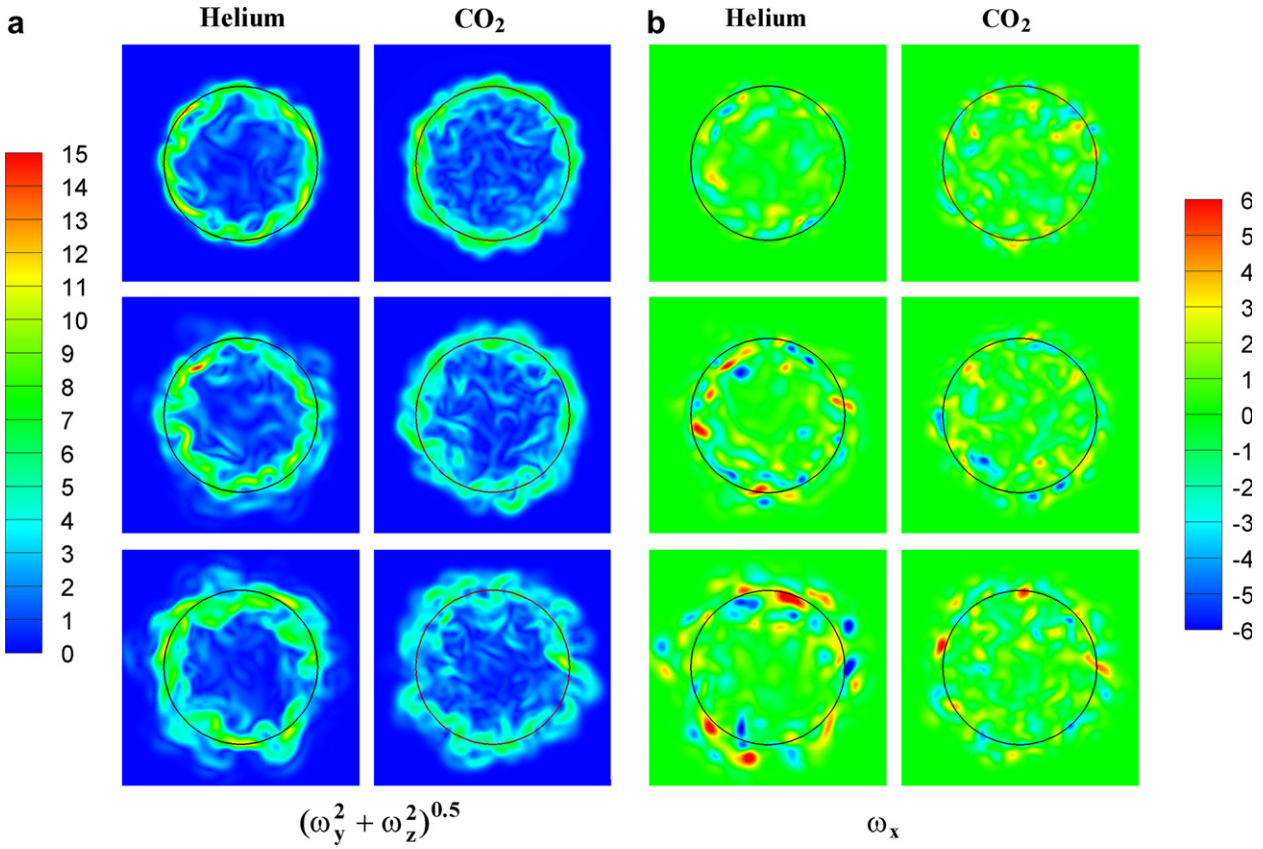

Fig. 14. Snapshots of the $(\omega_y^2 + \omega_z^2)^{0.5}$ and ω_x at three axial cross sections, $x/D_j = 0.4$, 0.8 and 1.2 from up to bottom, respectively.

and the CO_2 jet. A local maximum of $\langle \Omega_{x/yz} \rangle$ of 1.15 is found at $x/D_j = 0.088$, $r/D_j = 0.54$ while for air the maximum is 0.73 and for CO_2 0.72, respectively, attained at the same radial position and slightly lower x. This reflects a higher contribution from streamwise vorticity to the whole vorticity modulus. It is worth pointing out that the

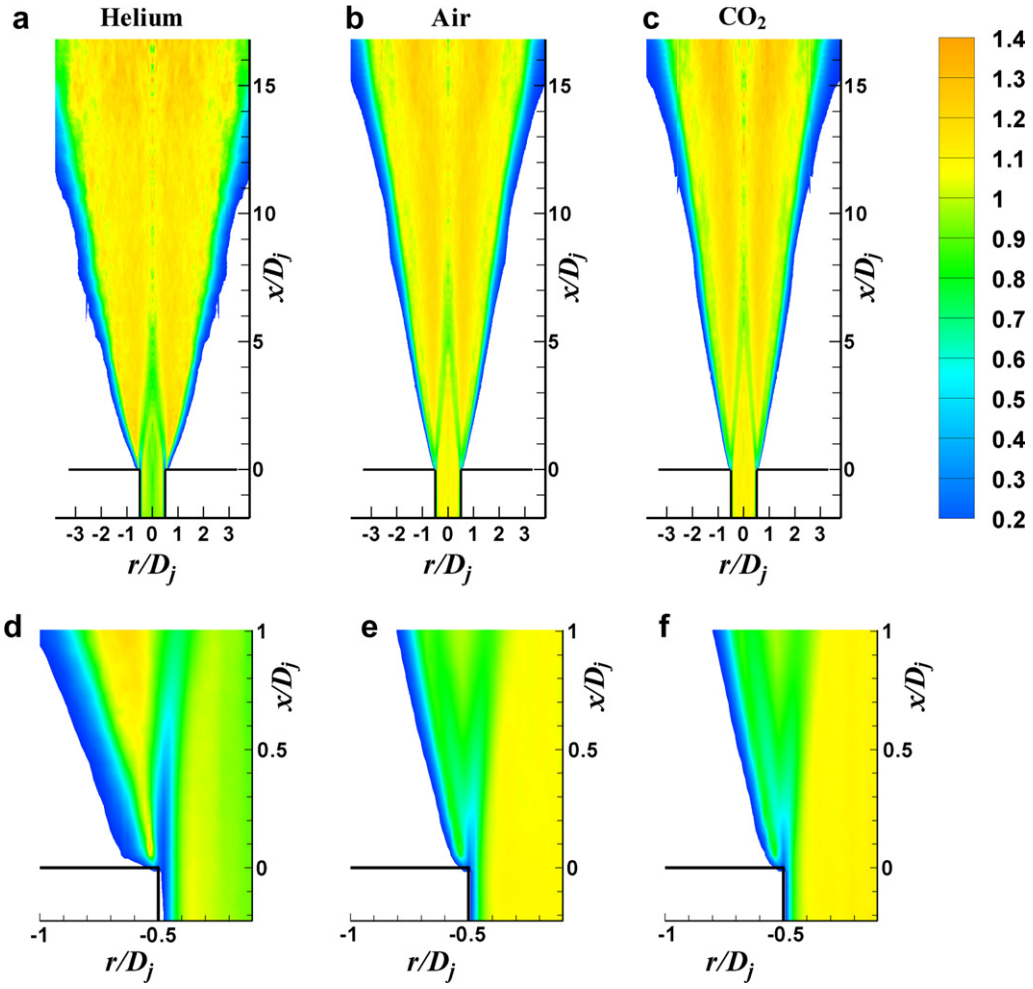

Fig. 15. Average value of $\Omega_{x/yz}$ in the center plane. (d), (e) and (f) is the zoom view of (a), (b) and (c), respectively.

vorticity and its components shown in Figs. 13–15 are all normalized with U_j/D_j. This excludes the possibility that the stronger contribution of streamwise vorticity for the Helium jet is due to the higher absolute inlet jet velocity.

6. Conclusions

Three weakly confined turbulent variable-density axisymmetric jets have been studied by LES. The density ratios range from 0.14 to 1.52. In the present paper, detailed comparison has been made for many statistical quantities, such as the axial evolution of mean streamwise velocity, turbulent intensities, as well as radial profiles of Reynolds stress. The agreement between simulation and experiment is generally very good. For the CO_2 jet the initial stages deviate somewhat, presumably due to imperfection in the experiment, but the downstream evolution is again well captured. Additionally, the effect of the density difference on the coherent structures in these jets is investigated. It is found that long finger-shaped streamwise vortices, regularly arranged along the jet nozzle lip, are produced in the helium jet, but not in the air and CO_2 jets. Furthermore, a characteristic quantity, which is used to detect the orientation of vorticity with respect to the jet axis is proposed and applied to the present cases. It reveals that there is a region with strong streamwise vorticity just beside the shear layer region in the helium jet, but not in the CO_2 jet. In the literature the occurrence of an absolute instability for low-density jets is discussed (Sreenivasan et al., 1989). The experiment was set up with conditions to avoid this regime (Djeridane et al., 1996). Whether or not such an instability occurs in the present helium jet could not be answered with the present data.

Acknowledgements

The authors gratefully acknowledge the support of the German Research Foundation (DFG) through the Collaborative Research Center SFB 606 'Unsteady Combustion'. The computations were performed on the HP-XC clusters of SSCK Karlsruhe, under project SFB606A6. F. Anselmet, Marseille, kindly provided the experimental data in electronic form.

References

Ahmed, S.A., So, R.M.C., Mongia, H.C., 1985. Density effects on jet characteristics in confined swirling flow. Exp. Fluids 3, 231–238.

Amielh, M., Djeridane, T., Anselmet, F., Fulachier, L., 1996. Velocity near-filed of variable density turbulent jets. Int. J. Heat Mass Transfer 39, 2149–2164.

Chen, C.J., Rodi, W., 1980. Vertical Turbulent Buoyant Jets—A Review of Experimental Data. The Science and Application of Heat and Mass Transfer. Pergamon Press, New York.

Djeridane, T., Amielh, M., Anselmet, F., Fulachier, L., 1996. Velocity turbulence properties in the near-field region of axisymmetric variable density jets. Phys. Fluids 8, 1614–1630.

Fulachier, L., Borchi, R., Anselmet, F., Paranthoen, P., 1989. Influence of density variations on the structures of low-speed turbulent flows: a report on Euromech 237. J. Fluid Mech. 203, 577–593.

García-Villalba, M., Fröhlich, J., Rodi, W., 2006. Identification and analysis of coherent structures in the near field of a turbulent unconfined annular swirling jet using large eddy simulation. Phys. Fluids 18, 055103.

Gharbi, A., Amielh, M., Anselmet, F., 1995. Experimental investigation of turbulence properties in the interface region of variable density jets. Phys. Fluids 7, 2444–2454.

Hinterberger, C., 2004. Dreidimensionale und Tiefenge-mittelte large-eddy-simulation von Flachwasser-strömungen. PhD Thesis. University of Karlsruhe, Germany.

Jester-Zürker, R., Jakirlić, S., Tropea, C., 2005. Computational modelling of turbulent mixing in confined swirling environment under constant and variable density conditions. Flow Turbul. Combust. 75, 217–244.

Moin, P., Squires, K., Cabot, W., Lee, S., 1991. A dynamic subgrid-scale model for compressible turbulence and scalar transport. Phys. Fluids A 3, 2746–2757.

Monkewitz, P.A., Lehmann, B., Barsikow, B., Bechert, D.W., 1989. The spreading of self-excited hot jets by side jets. Phys. Fluids A 1, 446–448.

Monkewitz, P.A., Pfizenmaier, E., 1991. Mixing by "side jets" in strongly forced and self-excited round jets. Phys. Fluids A 3, 1356–1361.

Panchapakesan, N.R., Lumley, J.L., 1993. Turbulence measurements in axisymmetric jets of air and helium—Part 2. Helium Jet. J. Fluid Mech. 246, 225–247.

Reinaud, J., Joly, L., Chassaing, P., 1999. Numerical simulation of a variable-density mixing-layer. In: Giovannini, A. et al. (Ed.), Proc. Third Int. Workshop on Vortex Flows and Related Numerical Methods, ESAIM, vol. 7, pp. 359–368.

Schowalter, D.G., Van Atta, C.W., Lasheras, J.C., 1994. Baroclinic generation of streamwise vorticity in a stratified shear layer. Meccanica 29, 361–371.

Sreenivasan, K.R., Raghu, S., Kyle, D., 1989. Absolute instability in variable density round jets. Exp. Fluids 7, 309–317.

Tyliszczak, A., Boguslawski, A., 2006. LES of the jet in low mach variable density conditions. In: Direct and Large-Eddy Simulation VI, Part XII. Springer, Netherlands, pp. 575–582.

Werner, H., Wengle, H., 1993. Large eddy simulation of turbulent flow over and around a cube in a plate channel. In: Proc. Eighth Symp. on Turbulent Shear Flows. Springer-Verlag, Berlin.

Widnall, S.E., Bliss, D.B., Tsai, C.Y., 1974. The instability of short waves on a vortex ring. J. Fluid Mech. 66, 35–47.

Zhou, X., Luo, K.H., Williams, J.J.R., 2001. Study of density effects in turbulent buoyant jets using large-eddy simulation. Theor. Comput. Fluid Dyn. 15, 95–120.

Zhu, J., 1991. A low diffusive and oscillation-free convection scheme. Commun. Appl. Num. Meth. 7, 225–232.